

Supporting Information

Field-induced single-ion magnet based on a quasi-octahedral Co(II) complex with mixed sulfur-oxygen coordination environment

D.V. Korchagin,^{*a} Ya.E. Gureev,^b E.A. Yureva,^a G.V. Shilov,^a A.V. Akimov,^a E.Ya. Misochko,^a R.B. Morgunov,^a K.V. Zakharov,^b A.N. Vasiliev,^{b,c} A.V. Palii,^{a,d} T. Lohmiller,^e K. Holldack^f and S.M. Aldoshin^a

-
- a. Institute of Problems of Chemical Physics, Russian Academy of Sciences, 1, Acad. Semenov Av., Chernogolovka, Russian Federation, 142432, * E-mail: korden@icp.ac.ru
- b. M.V. Lomonosov Moscow State University, Moscow 119991, Russia.
- c. National University of Science and Technology “MISiS”, Moscow, 119049, Russia
- d. Institute of Applied Physics, Academy of Sciences of Moldova, Kishinev, Moldova
- e. EPR4Energy Joint Lab, Department Spins in Energy Conversion and Quantum Information Science, Helmholtz-Zentrum Berlin für Materialien und Energie GmbH, 12489 Berlin, Germany
- f. Institut für Methoden und Instrumentierung der Forschung mit Synchrotronstrahlung, Helmholtz-Zentrum Berlin für Materialien und Energie GmbH, 12489 Berlin, Germany

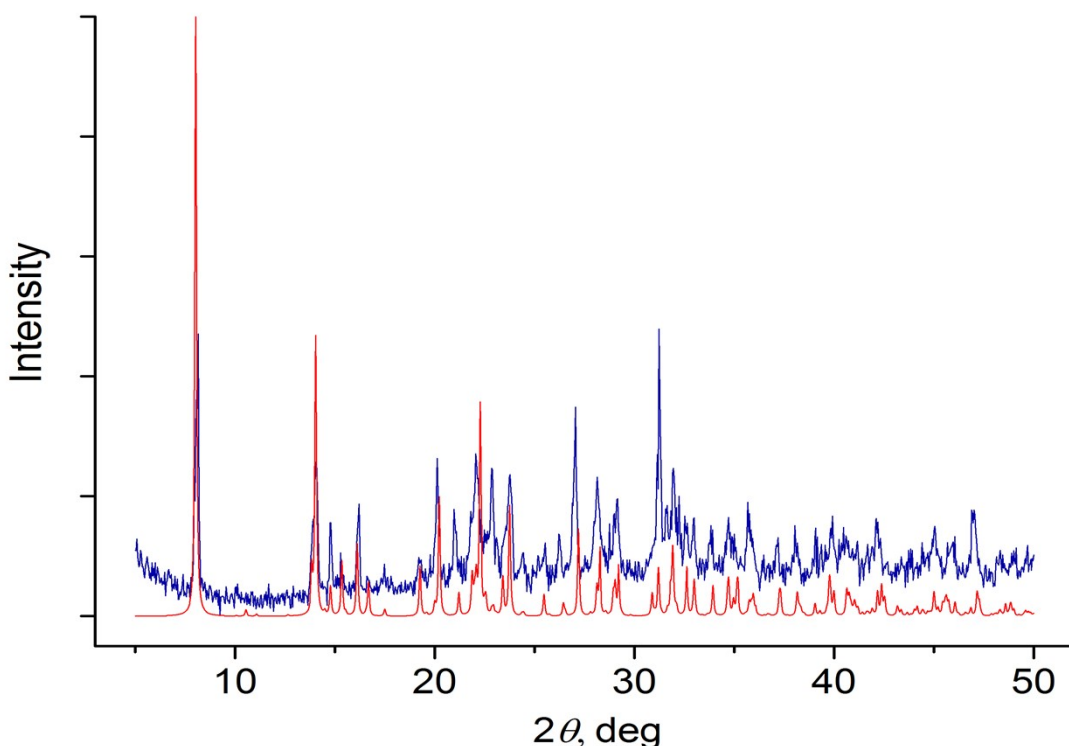


Figure S1. Powder X-ray diffraction pattern of polycrystalline sample of complex I: experimental (blue), and calculated from single crystal data (red).

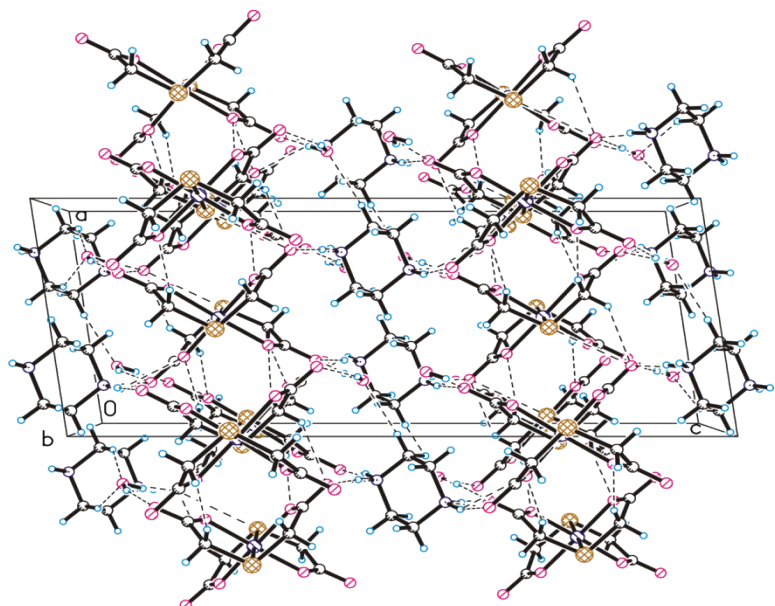


Figure S2. *ac* projection of the fragment of the crystal structure of **I**. Dashed lines show intermolecular hydrogen bonds.

Table S1. Crystal data and structure refinement for compound **I**.

Parameter	I
formula (<i>M</i>)	C ₁₂ H ₂₄ CoS ₂ N ₂ O ₁₀ (479.38)
crystal system, space group	monoclinic, <i>P</i> 2 ₁ / <i>n</i>
<i>a</i> , Å	9.1095(8)
<i>b</i> , Å	9.0580(6)
<i>c</i> , Å	22.1933(15)
β, deg.	97.765(6)
<i>V</i> , Å ³	1814.5(2)
<i>Z</i> , <i>d</i> _{calc} /g•cm ⁻³	4, 1.755
μ/mm ⁻¹	1.233
crystal size, mm	0.2 x 0.2 x 0.05
θ range for data collection, deg.	2.91 - 26.32
completeness to θ, %	99.9
reflections collected / unique	7714 / 3690 [<i>R</i> (<i>int</i>)=0.0269]
reflections [<i>I</i> > 2σ(<i>I</i>)]	2519
parameters	340
<i>R</i> ₁ (<i>wR</i> ₂) [<i>I</i> >2σ(<i>I</i>)]	0.0331 (0.0726)
<i>R</i> ₁ (<i>wR</i> ₂)	0.0419 (0.0762)
<i>GOF</i> (<i>F</i> ²)	1.066

Table S2. The bond lengths and angles in the structure of compound I.

Bond	d, Å	Bond	d, Å
Co(1)-O(1)	2.061(2)	Co(1)-O(2)	2.043(2)
Co(1)-O(3)	2.047(2)	Co(1)-O(4)	2.064(2)
Co(1)-S(1)	2.4781(7)	Co(1)-S(2)	2.4823(7)
S(1)-C(2)	1.801(2)	S(1)-C(4)	1.804(2)
S(2)-C(8)	1.802(2)	S(2)-C(6)	1.803(2)
C(2)-C(1)	1.517(3)	C(4)-C(3)	1.523(3)
C(6)-C(5)	1.519(3)	C(7)-C(8)	1.522(3)
O(1)-C(1)	1.253(3)	O(2)-C(3)	1.268(3)
O(5)-C(1)	1.257(3)	O(6)-C(3)	1.249(3)
O(3)-C(5)	1.258(3)	O(4)-C(7)	1.256(3)
O(7)-C(5)	1.257(3)	O(8)-C(7)	1.253(3)
N(1)-C(9)	1.494(3)	N(1)-C(12)	1.488(3)
N(2)-C(10)	1.492(3)	N(2)-C(11)	1.493(3)
C(9)-C(10)	1.511(3)	C(12)-C(11)	1.515(3)
Angle	ω, °	Angle	ω, °
O(1)-Co(1)-O(4)	178.19(6)	O(2)-Co(1)-O(3)	178.62(6)
O(2)-Co(1)-O(1)	92.52(6)	O(3)-Co(1)-O(4)	92.13(6)
O(3)-Co(1)-O(1)	86.13(6)	O(2)-Co(1)-O(4)	89.22(6)
O(1)-Co(1)-S(1)	82.32(5)	O(2)-Co(1)-S(1)	83.42(5)
O(3)-Co(1)-S(1)	96.12(5)	O(4)-Co(1)-S(1)	98.37(5)
O(1)-Co(1)-S(2)	96.90(5)	O(2)-Co(1)-S(2)	97.23(5)
O(3)-Co(1)-S(2)	83.21(5)	O(4)-Co(1)-S(2)	82.39(5)
C(2)-S(1)-C(4)	103.1(1)	C(8)-S(2)-C(6)	102.6(1)
C(2)-S(1)-Co(1)	96.06(8)	C(8)-S(2)-Co(1)	96.08(8)
C(4)-S(1)-Co(1)	95.36(8)	C(6)-S(2)-Co(1)	95.30(8)
C(1)-O(1)-Co(1)	124.0(2)	C(5)-O(3)-Co(1)	123.3(2)
C(3)-O(2)-Co(1)	123.5(2)	C(7)-O(4)-Co(1)	124.0(2)
C(12)-N(1)-C(9)	111.3(2)	C(10)-N(2)-C(11)	112.0(2)
C(1)-C(2)-S(1)	116.0(2)	C(5)-C(6)-S(2)	116.3(2)
C(3)-C(4)-S(1)	116.8(2)	C(7)-C(8)-S(2)	116.2(2)
O(1)-C(1)-O(5)	123.7(2)	O(6)-C(3)-O(2)	123.6(2)
O(7)-C(5)-O(3)	123.3(2)	O(8)-C(7)-O(4)	123.9(2)
O(7)-C(5)-C(6)	115.2(2)	O(8)-C(7)-C(8)	115.2(2)
O(3)-C(5)-C(6)	121.4(2)	O(4)-C(7)-C(8)	120.8(2)
O(1)-C(1)-C(2)	121.0(2)	O(2)-C(3)-C(4)	120.7(2)
O(5)-C(1)-C(2)	115.3(2)	O(6)-C(3)-C(4)	115.7(2)
N(1)-C(9)-C(10)	110.1(2)	N(2)-C(11)-C(12)	110.9(2)
N(1)-C(12)-C(11)	110.1(2)	N(2)-C(10)-C(9)	109.8(2)
S(1)-Co(1)-S(2)	179.01(2)		

Table S3. Geometric characteristics of intermolecular H-bonds in the crystal structure of compound I.

D-H	d(D-H)	d(H..A)	<DHA	d(D..A)	A
N(2)-H(4)	0.94	1.81	168.9	2.74	O(8) [-x+2, -y+1, -z+1]
O(2W)-H(7)	0.86	1.98	161.0	2.81	O(7) [x+1/2, -y+1/2, z+1/2]
N(1)-H(2)	0.98	1.76	161.5	2.71	O(6)
O(1W)-H(5)	0.82	2.19	154.1	2.95	O(6)[x, y+1, z]
O(1W)-H(6)	0.87	1.89	166.1	2.75	O(5) [-x+5/2, y+1/2, -z+1/2]
N(1)-H(1)	0.91	1.84	173.6	2.74	O(5) [-x+5/2, y+1/2, -z+1/2]
O(2W)-H(8)	0.87	2.03	160.8	2.87	O(8) [-x+2, -y, -z+1]
N(2)-H(3)	0.96	1.73	171.4	2.68	O(7) [x+1/2, -y+1/2, z+1/2]

Table S4. Best fit parameters of the two-component Debye model for the Cole-Cole plot of complex **I** at $H_{DC} = 1000$ Oe

T, K	$\chi_s, \text{cm}^3 \text{ mol}^{-1}$	$\Delta\chi_T, \text{cm}^3 \text{ mol}^{-1}$	τ, s	α	R_1^a
1.8	1.31	1.73	1.29E-03	0.24	3.51E-03
1.9	1.26	1.67	1.20E-03	0.26	2.95E-03
2.0	1.18	1.59	1.12E-03	0.27	2.60E-03
2.1	1.15	1.55	1.06E-03	0.27	1.95E-03
2.5	0.98	1.36	7.90E-04	0.26	1.13E-03
3.0	0.83	1.17	5.70E-04	0.22	4.27E-04
3.5	0.72	1.03	4.18E-04	0.22	5.73E-04
4.0	0.64	0.92	3.22E-04	0.19	5.53E-04
5.0	0.54	0.76	2.46E-04	0.13	1.72E-04

^a The mean residual sum of squares, $R_1 = \frac{1}{n} \sum_{i=1}^n \frac{(Y_{\text{exp}} - Y_{\text{calc}})^2}{Y_{\text{exp}}^2}$.

X-band EPR spectroscopy.

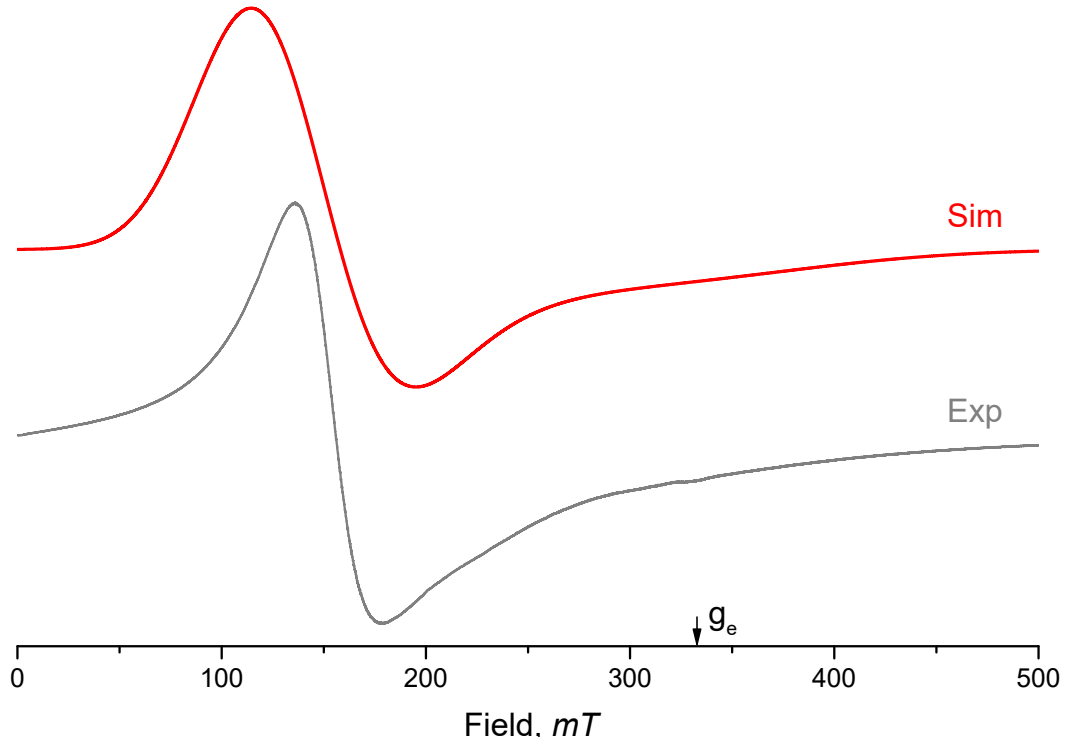


Figure S3. The X-band CW EPR spectrum of the powder sample of **I** at 5K (gray). Simulated spectrum (red) for magnetic parameters of **I** from SA-CASSCF/NEVPT2 quantum chemical calculations $S=3/2$, $D = + 54.76 \text{ cm}^{-1}$, $E/D = 0.082$, $\mathbf{g} = [2.46 \ 2.37 \ 1.99]$, $A(3/2) = [180 \ 211 \ 300] \text{ MHz}$, only the line width was adjusted.

FD-FT THz-EPR

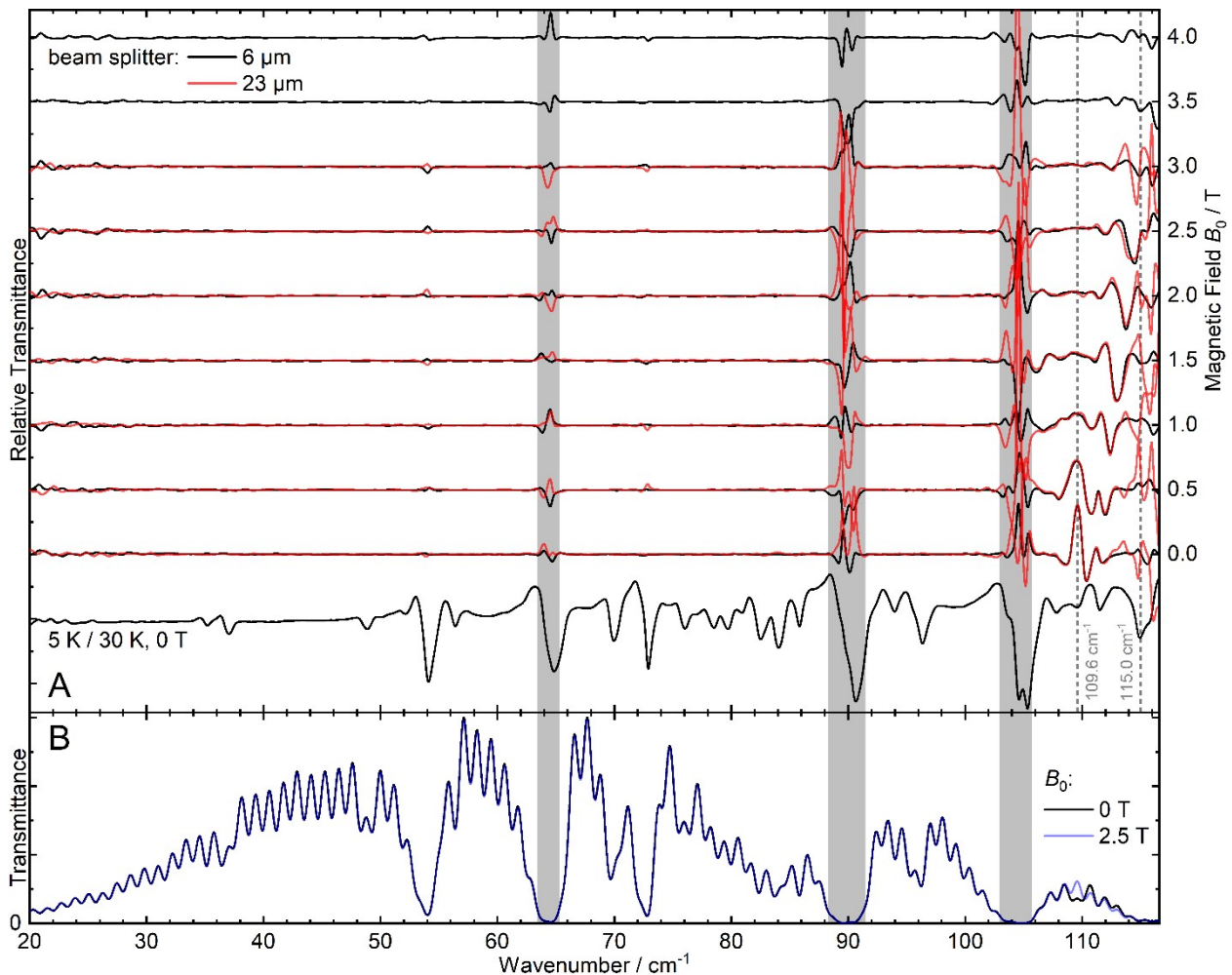


Figure S4. FD-FT THz-EPR spectra of **I**. (A) The bottom trace is a temperature division spectrum at zero-field obtained by dividing a raw transmission spectrum recorded at 5 K by one recorded at 30 K. Thus, maxima correspond to stronger absorption at 5 K, while minima correspond to more intense absorption at 30 K. The traces above are magnetic-field division spectra (MDS) recorded at 5 K obtained by division of a raw spectrum at $B_0 + 0.5$ T (0.5-4.5 T) by one measured at B_0 (0.0-4.0 T). Maxima correspond to stronger absorption at lower B_0 , minima to increased absorption at higher B_0 . The spectra were recorded using beam splitters of either 6 μm (black traces) or 23 μm (red traces) thickness, the former one enhancing light intensities at the high energy end compared to the latter one. Comparison of the MDS acquired with the different beam splitters proofs the authenticity of the EPR signal features centered at 109.6 cm^{-1} and observed in a range delimited by strong vibronic absorptions at 105.3 and 115.0 cm^{-1} . (B) Raw transmittance spectra of the pellet sample acquired at magnetic fields of 0 and 2.5 T. Intense absorption by vibronic transitions in compound **I** leads to transmittance approaching zero in the grey shaded areas and at energies beyond the spectral range depicted, thus introducing strong noise in the division spectra.